

Momentum transfer squared dependence of exclusive quarkonia photoproduction in UPCs

Cheryl Henkels^{1,*}, Emmanuel G. de Oliveira^{1,†}, Roman Pasechnik^{1,2,‡}, and Haimon Trebien^{1,§}

¹*Departamento de Física, CFM, Universidade Federal de Santa Catarina,
C.P. 476, CEP 88.040-900, Florianópolis, SC, Brazil*

²*Department of Astronomy and Theoretical Physics,
Lund University, SE-223 62 Lund, Sweden*

Abstract

In this paper, we study fully differential quarkonia photoproduction observables in ultraperipheral collisions (UPCs) as functions of momentum transfer squared. We employ the dipole picture of the QCD part of the scattering with proton and nucleus targets, with the projectile being a quasi-real photon flux emitted by an incoming hadron. We analyse such observables for ground J/ψ , $\Upsilon(1S)$ and excited ψ' , $\Upsilon(2S)$ states whose Light-Front wave functions are obtained in the framework of interquark potential model incorporating the Melosh spin transformation. Two different low- x saturation models, one obtained by solving the Balitsky–Kovchegov equation with the collinearly improved kernel and the other with a Gaussian impact-parameter dependent profile, are used to estimate the underlined theoretical uncertainties of our calculations. The results for the proton target and with charmonium in the final state are in agreement with the available HERA data, while in the case of nucleus target we make predictions for γA and AA differential cross sections at different W and at $\sqrt{s} = 5.02$ TeV, respectively.

PACS numbers: 14.40.Pq,13.60.Le,13.60.-r

* cherylhenkels@hotmail.com

† emmanuel.de.oliveira@ufsc.br

‡ Roman.Pasechnik@thep.lu.se

§ haimontrebien@outlook.com

I. INTRODUCTION

The determination of the structure of protons and nuclei in terms of their fundamental constituents as well as their interactions is one of the biggest goals of particle physics [1]. An important milestone for the proton structure measurements was the start of operation of the HERA collider at DESY. There, a large amount of Deep Inelastic Scattering (DIS) data (in which simple point-like leptons are used to probe the proton substructure) has been collected, making it possible to extract a detailed knowledge about the parton distribution functions (PDFs) for the proton with a good precision for as low longitudinal momentum fraction x as 10^{-5} or so [2].

In order to obtain a more detailed picture of the target, in particular, to access an information about its transverse shape at a given x , more differential observables are needed. Two processes that provide such observables, the DVCS (where the outgoing photon is real) and the exclusive production of vector mesons (with the same quantum numbers $J^{PC} = 1^{--}$ as those of the photon), are frequently discussed in the literature. In the first case, thanks to the high beam energy available at the HERA collider, the experiments H1 and ZEUS have measured the pure DVCS cross section for the Bjorken variable ranging between 10^{-4} and 10^{-2} . In the second case, besides exclusive electro- and photoproduction of light vector mesons (ϕ , ρ) and quarkonia (J/ψ) studied by the H1 and ZEUS collaborations, there are more recent data on vector meson photoproduction in ultraperipheral collisions (UPCs) available from the LHC. The latter processes are in the main focus of this work.

Particle production processes in proton-nucleus pA and nucleus-nucleus AA UPCs have attracted a lot of attention in recent years due to their vast potential in probing the proton and nucleus structure at very small x (for a recent review, see e.g. Ref. [3]). A particularly clean environment in UPCs is achieved in a fully exclusive process when a small-mass hadronic system is produced being separated from the intact scattered particles by large rapidity gaps on both sides. A phenomenologically important and well-known example of such a scattering refers to exclusive quarkonia (such as charmonia $J/\psi \equiv \psi(1S)$, $\psi' \equiv \psi(2S)$) and bottomonia $\Upsilon(1S, 2S)$) photoproduction reactions in UPCs that has recently gained a particular relevance motivated by a wealth of experimental data coming from the LHC, such as those from LHCb [4–6], ALICE [7–11] and CMS [12, 13] experiments.

The process is straightforwardly visualised by considering it in the target rest frame. While on one side of the collision, a photon flux is being emitted from a fast projectile (hadron or nucleus) and then fluctuate into a color-neutral $Q\bar{Q}$ ($Q = c, b$) pair called a color dipole, on another side such a dipole coherently rescatters off the target by means of an exchange of multiple gluonic system in a color-singlet state – a dominating configuration at low longitudinal momentum transfers, x . In the leading-order perturbative Quantum Chromodynamics (QCD) approximation, typically validated by having a hard scale associated with the heavy-quark mass m_Q , one considers a colorless gluon-pair exchange between the dipole and the target. In the limit of small $x \ll 1$ and low four-momentum transfer squared $|t| = -(p_1 - p'_1)^2 \ll m_Q^2$, such an exchange in momentum space is usually described in terms of the generalised unintegrated gluon density in the target which, in turn, connects to the dipole scattering matrix as a function of gluon x , dipole separation \vec{r} and the impact parameter of the scattering \vec{b} . This matrix effectively encodes dynamics of parton saturation as well as contains full information about the relative dipole orientation with respect to the color background field of the target. As long as \vec{r} is integrated out in a convolution with the quarkonium light-front (LF) wave function, the impact parameter dependence provides the

transverse profile of the target gluon density that can be probed by means of the measured differential in t distributions.

The impact-parameter dependence of the gluon density in the target is an intrinsically non-perturbative property and is often parameterised in terms of a Gaussian distribution like it is done, for example, in the case of the so-called “bSat” model [14]. In order to get a more accurate description of interactions between the color dipole and the target encoded in the impact-parameter profile of the target, the corresponding amplitude can be found by solving the Balitsky-Kovchegov (BK) evolution equation [15, 16]. It is known that the BK equation at the next-to-leading order (NLO) is unstable due to large NLO corrections when one integrates out the gluon emissions with small transverse momenta. So, these corrections need to be properly resummed to all orders [17]. Besides, an additional phenomenon called the Coulomb tails that corresponds to an unphysical growth of the amplitude at large impact parameters should be taken into consideration. The latter phenomenon is found to be connected to the creation of large daughter dipoles during the evolution, thus enabling this problem to be cured. The BK solutions without such Coulomb tails can be found in several recent studies, e.g. in Refs. [18, 19] this problem is absent by the use of the collinearly improved kernel. In the current analysis, we apply both the “bSat” model and the BK solution with collinearly improved kernel in the study of differential quarkonia photoproduction cross sections in UPCs for relevant experimental conditions at HERA and LHC colliders.

The paper is organised as follows. In Sect. II, we give a short description of the differential cross section of elastic vector meson photoproduction $\gamma p \rightarrow Vp$ off the proton target in terms of the dipole S -matrix and quarkonia LF wave functions in the framework of potential approach. In Sect. III, we discuss the models for the impact-parameter dependent partial dipole amplitude that have been used in the numerical analysis throughout this work. Sect. IV presents the numerical results for the differential cross section of the $\gamma p \rightarrow Vp$ process for the ground and excited quarkonia states, with J/ψ results successfully describing the existing data. In Sect. V, we review the formalism to obtain the differential cross section of coherent quarkonia photoproduction off nuclear targets in UPCs and show our corresponding numerical predictions for the ground and first excited ψ and Υ states presented in Sect. VI. At last, a brief summary of our results is given in Sect. VII.

II. ELASTIC PHOTOPRODUCTION OFF A PROTON

The advantage of studying the vector meson photoproduction is that, in order to produce a single vector meson and nothing else in a detector, a color charge cannot be transferred to the target, requiring that at least two gluons (in the net color-singlet state) are exchanged. This provides an exclusive character of the process, with a particularly clean environment. Another advantage is that only in the exclusive scattering process it is possible to measure the total momentum transfer Δ_T , and interpret it as the Fourier conjugate of the impact parameter. Consequently, these processes probe not only the density of partons, but also their spatial distribution in the transverse plane.

Considering first the proton target case, at high energies the elastic diffractive differential cross section for the $\gamma p \rightarrow Vp$ scattering is found as follows [14]:

$$\frac{d\sigma^{\gamma p \rightarrow Vp}}{dt} = \frac{1}{16\pi} |\mathcal{A}^{\gamma p}(x, \Delta_T)|^2, \quad (2.1)$$

where $t = -\Delta_T^2 \equiv (p_1 - p'_1)^2$ is the momentum transfer squared, $\Delta_T \equiv |\mathbf{\Delta}|$ is the trans-

verse momentum of the produced vector meson V recoiled against the target (assuming the projectile photon momentum to be collinear i.e. carries no transverse momentum), and the elastic production amplitude

$$\mathcal{A}^{\gamma p}(x, \Delta_T) = \int d^2\mathbf{r} \int_0^1 dz (\Psi_V^* \Psi_\gamma) \mathcal{A}_{q\bar{q}}(x, \mathbf{r}, \Delta), \quad (2.2)$$

is given in terms of the overlap between the transversely-polarised real photon $\gamma \rightarrow Q\bar{Q}$ (Ψ_γ) and vector meson $V \rightarrow Q\bar{Q}$ LF wave functions (Ψ_γ and Ψ_V , respectively). Here, the elementary amplitude for elastic $q\bar{q}$ dipole scattering $\mathcal{A}_{q\bar{q}}$ is related to the dipole S -matrix

$$\mathcal{A}_{q\bar{q}}(x, \mathbf{r}, \Delta) = \int d^2\mathbf{b} e^{-i\mathbf{b}\cdot\Delta} \mathcal{A}_{q\bar{q}}(x, \mathbf{r}, \mathbf{b}) = i \int d^2\mathbf{b} e^{-i\mathbf{b}\cdot\Delta} 2[1 - S(x, \mathbf{r}, \mathbf{b})]. \quad (2.3)$$

and thus contains the most detailed (5-dimensional) information about the gluons density in the target. It is directly connected to the so-called gluon Wigner distribution as was established earlier in Ref. [20]. Even though a direct access of the elliptic gluon density in the Wigner distribution by a measurement of the exclusive quarkonia photoproduction is impossible, due \mathbf{r} variable being integrated in the measured differential cross section, an access of the impact parameter profile of the target gluon density is still very relevant for understanding the hadron or nucleus structure at very low momentum transfers.

Note, by means of the optical theorem, the imaginary part of the partial dipole amplitude in the forward limit ($\Delta_T \rightarrow 0$) is related to the dipole cross section $\sigma_{q\bar{q}}(x, r)$ – a universal ingredient whose parameterization can be extracted from a given process (typically, from DIS) and then used for description of many other processes in ep , pp and pA collisions [21, 22] (for a first analysis of elastic charmonia photoproduction in the dipole picture, see e.g. Refs. [23–27]).

In the off-forward case, one straightforwardly rewrites the elastic amplitude in terms of the imaginary part of the elastic $q\bar{q}$ amplitude in the impact parameter representation in the following way [14]

$$\mathcal{A}^{\gamma p}(x, \Delta_T) = 2i \int d^2\mathbf{r} \int_0^1 dz \int d^2\mathbf{b} (\Psi_V^* \Psi) e^{-i[\mathbf{b} - (1-z)\mathbf{r}] \cdot \Delta} N(x, \mathbf{r}, \mathbf{b}). \quad (2.4)$$

where z is the longitudinal momentum fraction of a heavy (anti)quark in the $Q\bar{Q}$ dipole, and

$$N(x, \mathbf{r}, \mathbf{b}) \equiv \text{Im}\mathcal{A}_{q\bar{q}}(x, \mathbf{r}, \mathbf{b}) = 2[1 - \text{Re}S(x, \mathbf{r}, \mathbf{b})], \quad (2.5)$$

such that the dipole cross section is defined as follows,

$$\sigma_{q\bar{q}}(x, r) = 2 \int d^2\mathbf{b} N(x, \mathbf{r}, \mathbf{b}). \quad (2.6)$$

In order to take into account the real part of the $\mathcal{A}_{q\bar{q}}$ amplitude, it suffices to introduce in Eq. (2.1) a factor that represents the ratio of the real to imaginary parts of the exclusive photoproduction amplitude $\mathcal{A}^{\gamma p}$ as follows [28]:

$$\mathcal{A}^{\gamma p} \Rightarrow \mathcal{A}^{\gamma p} \left(1 - i \frac{\pi\lambda}{2} \right), \quad \text{with} \quad \lambda = \frac{\partial \ln \mathcal{A}^{\gamma p}}{\partial \ln(1/x)}. \quad (2.7)$$

At last, one typically also incorporates the so-called skewness effect of the off-diagonal gluon distribution, which takes into account the fact that the gluons exchanged between the $q\bar{q}$ pair and the target can carry very different fractions of the target's momentum (x and x'), while in the dipole cross section parameterisations fitted to the inclusive DIS data they appear to be same due to the optical theorem. So, considering the dominant kinematical configuration with $x' \ll x \ll 1$, the skewness effect is typically included via a multiplicative factor R_g^2 applied to the differential cross section in Eq. (2.1) (see e.g. Ref. [29]), with

$$R_g(\lambda) = \frac{2^{2\lambda+3} \Gamma(\lambda + 5/2)}{\sqrt{\pi} \Gamma(\lambda + 4)}, \quad (2.8)$$

where λ is found in Eq. (2.7).

Following our previous work [30], we have used the vector-meson wave functions calculated within the potential approach, which relies on factorisation of the wave function into the spin-dependent and radial components. In the rest frame of the color dipole, the radial wave function is found as a numerical solution of the Schrödinger equation, which can be solved for different models for the interquark potential and then boosted to the infinite momentum frame, where the dipole formula for the vector meson production amplitude (2.4) is defined. In this analysis, we utilise five different models for the $Q\bar{Q}$ ($Q = c, b$) interaction potential: power-like model [31, 32] (pow), harmonic oscillator (osc), Cornell potential [33, 34] (cor), Buchmüller-Tye parametrisation [35] (but) and logarithmic potential [36] (log). The short-distance amplitudes have been computed with the fixed quark mass values $m_c = 1.4$ GeV and $m_b = 4.75$ GeV for charm and bottom quarks, respectively.

When performing the Lorentz transformation between the two frames, not only the radial part should be properly boosted, but also the spin-dependent part has to be transformed accordingly. Such a transformation is known as the Melosh spin rotation of the quark spinors [37] which causes an important impact on the differential photoproduction cross section, especially for excited quarkonia states [38, 39] (for a detailed analysis of the Melosh spin rotation effect, see Refs. [28]). Indeed, the spin rotation increases the ground-state quarkonia cross sections by approximately 30%, while for the excited states the increase is by a factor of 2-3 playing an important role in description of the exclusive vector meson photoproduction data.

Using such a quarkonium wave function in Eq. (2.4), the resulting photoproduction amplitude (considering the transversely-polarised real photon only) is given by

$$\begin{aligned} \mathcal{A}_{T,L}^{\gamma p}(x, \Delta_T) = & 2i \int d^2\mathbf{r} \int_0^1 dz \int d^2\mathbf{b} e^{-i[\mathbf{b} - (1-z)\mathbf{r}] \cdot \mathbf{\Delta}} \\ & \times [\Sigma^{(1)}(z, r)N(x, \mathbf{r}, \mathbf{b}) + \Sigma^{(2)}(z, r)N'_r(x, \mathbf{r}, \mathbf{b})], \end{aligned} \quad (2.9)$$

where $N'_r \equiv dN/dr$,

$$\Sigma^{(1)} = \frac{Z_Q \sqrt{N_c \alpha_{\text{em}}}}{2\pi\sqrt{2}} 2K_0(m_{QR}) \int dp_T J_0(p_T r) \Psi_V(z, p_T) p_T \frac{m_T m_L + m_T^2 - 2z(1-z)p_T^2}{m_L + m_T},$$

and

$$\Sigma^{(2)} = \frac{Z_Q \sqrt{N_c \alpha_{\text{em}}}}{2\pi\sqrt{2}} 2K_0(m_{QR}) \int dp_T J_1(p_T r) \Psi_V(z, p_T) \frac{p_T^2}{2} \frac{m_L + m_T + (1-2z)^2 m_T}{m_T(m_L + m_T)}.$$

Here, $\alpha_{\text{em}} = 1/137$ is the fine structure constant, $N_c = 3$ is the number of colors in QCD, Z_Q and m_Q are the electric charge and the mass of the heavy quark, respectively, $J_{0,1}$ (K_0) are the (modified) Bessel functions of the first (second) kind, respectively, p_T is the transverse momentum of the produced quarkonium state, and

$$m_T = \sqrt{m_Q^2 + p_T^2}, \quad m_L = 2m_Q \sqrt{z(1-z)}. \quad (2.10)$$

III. PARTIAL DIPOLE AMPLITUDE

For the main purpose of scanning of the impact-parameter profile of the target nucleon or nucleus, we need an impact-parameter dependent (or \mathbf{b} -unintegrated) dipole cross section that can be found in terms of the dipole S -matrix introduced in Eq. (2.3). First, we tested seven different models available from the literature, and then we selected the two that best describe the exclusive vector meson photoproduction data from the HERA collider, namely, the impact parameter dipole saturation model [14] (dubbed as “bSat” in what follows) and the model based upon a numerical solution of the Balitsky-Kovchegov (BK) equation [18].

In the first case of “bSat”, we employ the following formula

$$N(x, \mathbf{r}, \mathbf{b}) = 1 - \exp\left(-\frac{\pi^2}{2N_c} r^2 \alpha_s(\mu^2) xg(x, \mu^2) T(b)\right), \quad (3.1)$$

where $\mu^2 = 4/r^2 + \mu_0^2$ is the momentum scale in the collinear gluon density $xg(x, \mu^2)$, and no non-trivial information about the relative dipole orientation is implemented. In numerical calculations, we have used the CT14LO parameterisation [40] motivated by our earlier analysis of integrated quarkonia photoproduction cross sections performed in Ref. [30]. Besides, we considered a conventional Gaussian form for the proton shape function $T(b)$

$$T(b) = \frac{1}{2\pi B_G} e^{-b^2/2B_G}, \quad (3.2)$$

where the slope parameter $B_G = 4.25 \text{ GeV}^{-2}$ is found at Ref. [41].

In the second case, the numerical solution of the BK equation is provided by Ref. [18], where it is obtained under the assumption that the dipole partial amplitude depends only on the absolute values of the transverse separation of the dipole r and the impact parameter b , but does not depend on the angle between \mathbf{r} and \mathbf{b} similarly to the “bSat” model. In this case, the BK equation reads

$$\begin{aligned} \frac{\partial \mathcal{N}(r, b, Y)}{\partial Y} = & \int d^2 \mathbf{r}_1 K(r, r_1, r_2) \left(\mathcal{N}(r_1, b_1, Y) + \mathcal{N}(r_2, b_2, Y) - \mathcal{N}(r, b, Y) \right. \\ & \left. - \mathcal{N}(r_1, b_1, Y) \mathcal{N}(r_2, b_2, Y) \right) \end{aligned} \quad (3.3)$$

whose numerical solution provides us with the partial dipole amplitude

$$N(x, \mathbf{r}, \mathbf{b}) = \mathcal{N}(r, b, \ln(0.008/x)) \quad (3.4)$$

that has been employed in our numerical analysis below. The specific main feature of Ref. [18] solution is that it is obtained with a collinearly improved kernel $K(r, r_1, r_2)$ studied

in Ref. [42] that suppresses the larger daughter dipole sizes during the evolution and thus does not show the nonphysical Coulomb tails.

Finally, following Refs. [43–45], we also incorporate a correction relevant at large- x multiplying the dipole cross section by a factor $(1-x)^{2n_s-1}$, where n_s denotes the number of spectator quarks, which was chosen to be $n_s = 4$.

IV. RESULTS FOR $\gamma p \rightarrow Vp$ PROCESS

Now, that we have outlined the basic dipole formalism needed for analysis of the differential photoproduction observables, let us first present the numerical results for the $\gamma p \rightarrow Vp$ process. Note, in general the differential photoproduction cross sections computed for the proton target are very sensitive to the dipole parametrization used in the analysis. In this work, we analysed many different b -dependent parameterisations for the partial dipole amplitude, and they all give very different results. We chose to present the results obtained only with the BK solution and the “bSat” model briefly described above as those that provide the best description of the available J/ψ data. We will start with the BK solution model.

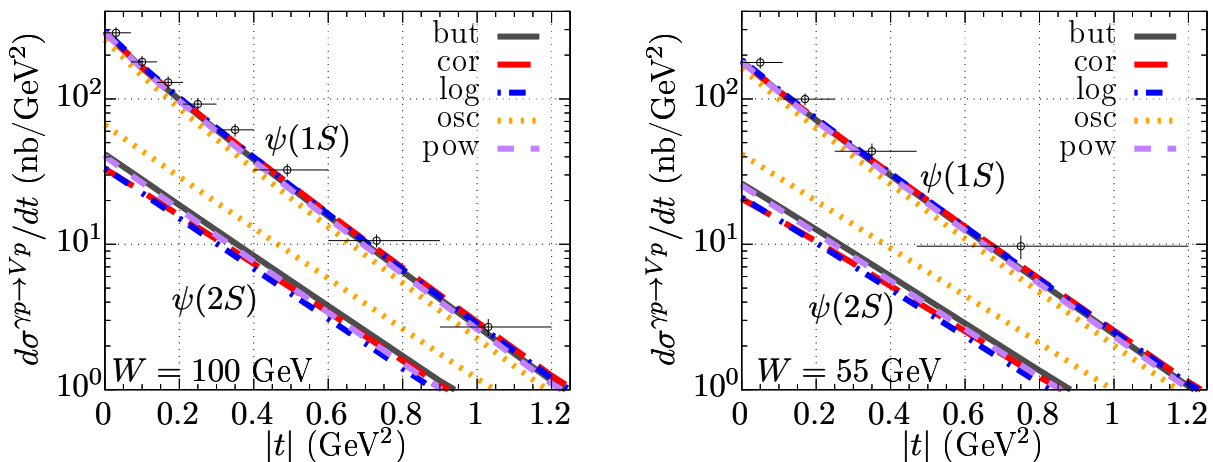


FIG. 1: Differential cross section for $\psi(1S)$ (upper curves) and $\psi(2S)$ (lower curves) as a function of $|t|$ obtained using the numerical solution of the BK equation obtained in Ref. [18], for $W = 100$ GeV (left) and $W = 55$ GeV (right). The results are presented for five different interquark potential models. The $\psi(1S)$ results are compared to the corresponding data from H1 Collaboration [46, 47].

Fig. 1 shows the differential cross section for $J/\psi \equiv \psi(1S)$ (upper curves) and $\psi(2S)$ (lower curves) production as a function of the momentum transfer squared $|t|$ for $W = 100$ GeV (left) and $W = 55$ GeV (right). Here, the results are obtained using a numerical solution of the BK equation of the b -dependent partial dipole amplitude discussed above. The ground-state charmonium results were compared to the experimental data available from the H1 Collaboration [46, 47] yielding a very good description. The corresponding observables have been evaluated with the LF quarkonia wave functions obtained for several different parametrizations of the interquark $Q\bar{Q}$ potential (for more details, see Refs. [30, 39]) which lead to a rather minor variation in the final results. A bigger difference is found for the $\psi(2S)$ cross section computed with the harmonic oscillator potential which is noticeably

higher than the results for other potentials. This effect is due to a specific shape of this wave function as was briefly discussed in Ref. [30]. The $|t|$ -slope is close to a constant due to an almost exponential impact parameter profile of the partial dipole amplitude, in full consistency with the J/ψ data. One notices however a somewhat larger difference in the slopes of J/ψ and $\psi(2S)$ differential cross sections due different shapes of the wave functions.

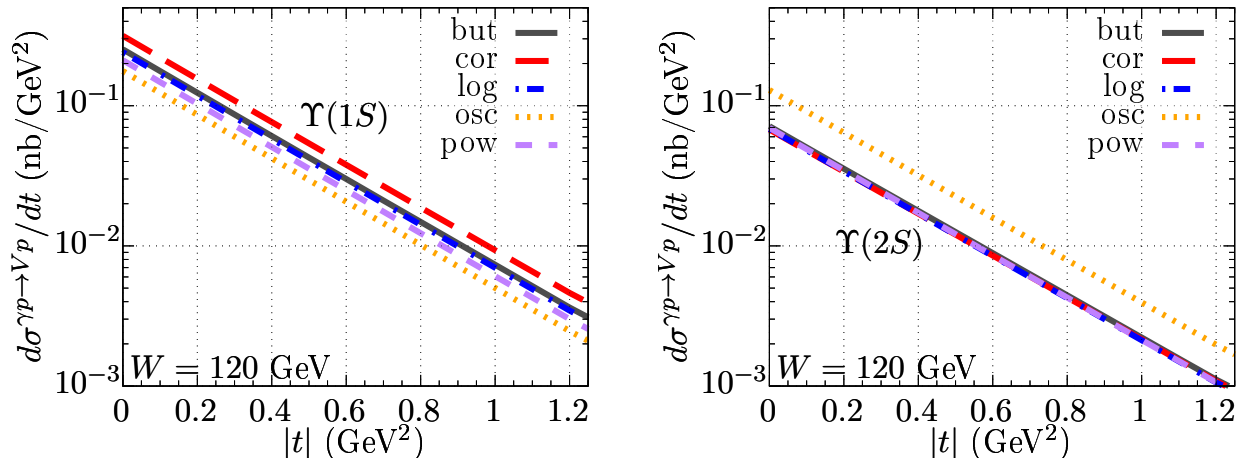


FIG. 2: Predictions for the differential cross section for $\Upsilon(1S)$ (left) and $\Upsilon(2S)$ (right) as a function of $|t|$ obtained using the numerical solution of the BK equation obtained in Ref. [18], for $W = 120$ GeV. The results are presented for five different interquark potential models.

In Fig. 2 we present our predictions for the differential cross section of $\Upsilon(1S)$ (left) and $\Upsilon(2S)$ (right) states as a function of $|t|$, also using the numerical solution of the BK equation, for $W = 120$ GeV. The results for the ground and excited states are separated into two different plots since the corresponding results for the oscillator potential are very close. This occurs due to the fact that these two wave functions in the case of harmonic oscillator have a very similar small- r dependence. Since this domain plays a dominant role in the integration of the Υ production amplitudes, one indeed arrives at very similar numerical results for $\Upsilon(1S)$ and $\Upsilon(2S)$ photoproduction in this case.

Figs. 3 and 4 represent the same quantities as in Figs. 1 and 2, respectively, except that the former are computed with the “bSat” dipole parameterisation instead of the BK solution employed in the latter. As can be seen in Fig. 3, the use of the “bSat” dipole model and the LF quarkonia wave functions calculated within the potential approach also provides a fair description of the H1 data. The latter is not as good as in case of the BK solution though. However, since “bSat” dipole parameterisation is widely used in the literature, in this work we chose to show the corresponding numerical results as well. A comparison between the curves obtained with these two dipole models and the available H1 data for $\psi(1S)$ photoproduction is presented in Fig. 5, where we can see that both curves found are mainly located within the experimental error bars for both $W = 100$ GeV (left) and $W = 55$ GeV (right), except that at small $|t|$ and at large W the “bSat” model marginally overshoots the data.

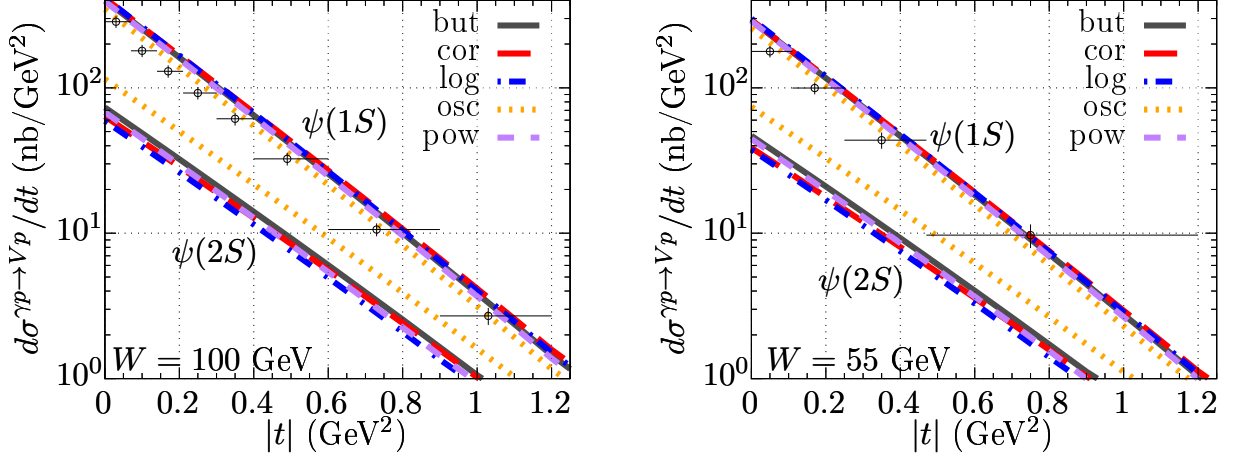


FIG. 3: Differential cross section for $\psi(1S)$ (upper curves) and $\psi(2S)$ (lower curves) as a function of $|t|$ found with the the “bSat” dipole model for $W = 100$ GeV (left) and $W = 55$ GeV (right), including also the skewness effect. The results are presented for five different interquark potential models. The $\psi(1S)$ results are compared to the corresponding data from H1 Collaboration [46, 47].

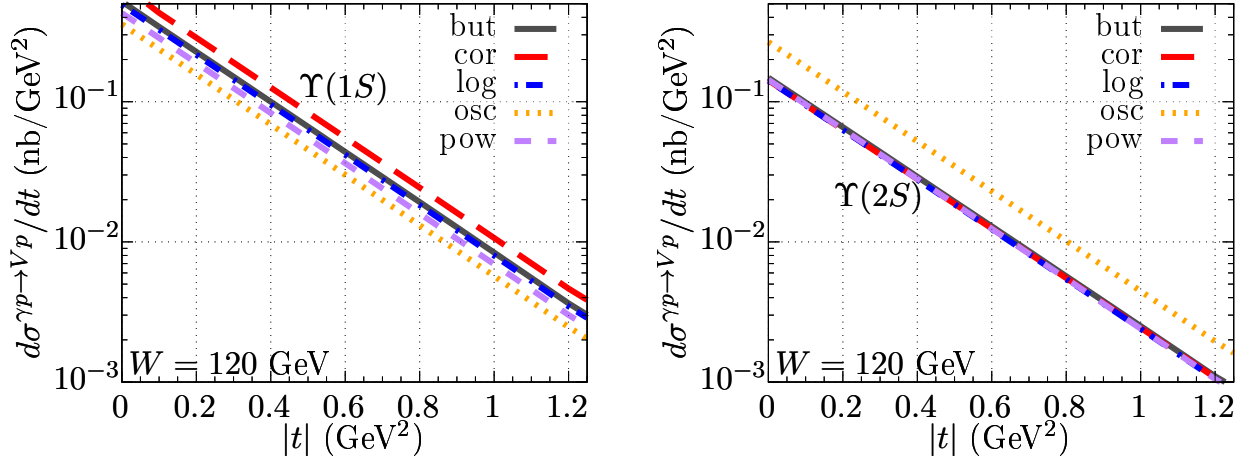


FIG. 4: Predictions for the differential cross section for $\Upsilon(1S)$ (left) and $\Upsilon(2S)$ (right) as a function of $|t|$ computed with the “bSat” dipole model for $W = 120$ GeV. The results are presented for five different interquark potential models.

V. COHERENT PHOTOPRODUCTION OFF NUCLEAR TARGETS

In photon-nucleus scattering, the differential cross section for coherent quarkonia V photoproduction $\gamma A \rightarrow VA$ off a nuclear target with atomic mass A can be found as follows:

$$\frac{d\sigma^{\gamma A \rightarrow VA}}{dt} = \frac{1}{16\pi} |\langle \mathcal{A}^{\gamma A}(x, \Delta_T) \rangle_N|^2, \quad (5.1)$$

in terms of the averaged amplitude [48]

$$\langle \mathcal{A}^{\gamma A} \rangle_N = 2i \int d^2\mathbf{r} \int_0^1 dz \int d^2\mathbf{b} e^{-i[\mathbf{b} - (1-z)\mathbf{r}] \cdot \Delta} \Sigma_T \langle N_A(x, \mathbf{r}, \mathbf{b}) \rangle_N, \quad (5.2)$$

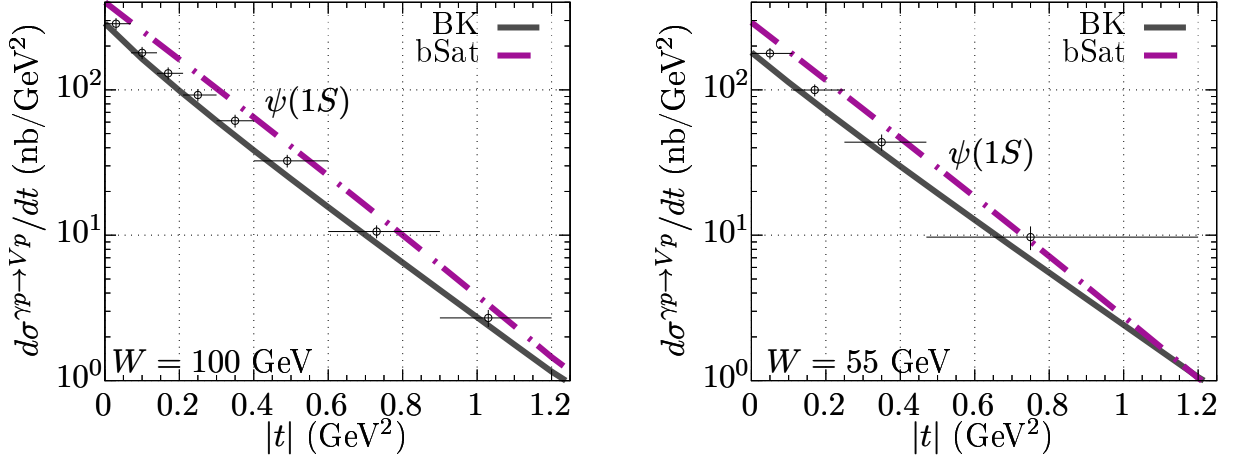


FIG. 5: Differential cross section for $\psi(1S)$ photoproduction as a function of $|t|$ found using the Buchmüller-Tye potential as well as the BK and “bSat” models for $W = 100$ GeV (left) and $W = 55$ GeV (right). The $\psi(1S)$ results are compared to the corresponding data from H1 Collaboration [46, 47].

where $\Sigma_T = \Sigma^{(1)} + \Sigma^{(2)}\partial/\partial r$, with the coefficients found in Eq. (2.9). Following Ref. [41], the dipole-nucleus scattering amplitude averaged over all possible configurations of the nucleons in the target nucleus reads

$$\langle N_A(x, \mathbf{r}, \mathbf{b}) \rangle_N = 1 - \left(1 - \frac{T_A(b)\sigma_{q\bar{q}}(x, r)}{2A} \right)^A. \quad (5.3)$$

This equation was obtained using a b dependent dipole amplitude parametrization, in the same way as above. It differs from other approach found in Ref. [49], where a Gaussian shape was assumed to describe such b dependence. The terms that appear in Eq. (5.3) are the usual (integrated) dipole cross section off the proton target, $\sigma_{q\bar{q}}(x, r)$, found in Eq. (2.6), and

$$T_A(b) = \int_{-\infty}^{+\infty} dz \rho_A(b, z), \quad \frac{1}{A} \int d^2b T_A(b) = 1, \quad (5.4)$$

being the thickness function of the nucleus given in terms of the normalised Woods-Saxon distribution [50],

$$\rho_A(b, z) = \frac{\mathcal{N}}{1 + \exp[\frac{r(b, z) - c}{\delta}]}, \quad r(b, z) = \sqrt{b^2 + z^2}. \quad (5.5)$$

Here, $r(b, z)$ is the distance from the center of the nucleus and \mathcal{N} is an appropriate normalisation factor. In this work, we consider UPCs of lead nuclei, with $A = 208$ and the parameters $c = 6.62$ fm and $\delta = 0.546$ fm are used [51].

The amplitude in Eq. (5.2) takes into account the imaginary part of the amplitude only. In order to incorporate the real part, one performs the following substitution,

$$\sigma_{q\bar{q}}(x, r) \Rightarrow \sigma_{q\bar{q}}(x, r) \left(1 - i \frac{\pi\lambda}{2} \right) \quad \text{with} \quad \lambda = \frac{\partial \ln \sigma_{q\bar{q}}(x, r)}{\partial \ln(1/x)}, \quad (5.6)$$

analogical to the one made for the proton target case in Eq. (2.7). Furthermore, in order to introduce a skewness correction to the associated nuclear gluon density, one can multiply the dipole cross section by the corresponding skewness factor found in Eq. (2.8) as

$$\sigma_{q\bar{q}}(r, x) \rightarrow \sigma_{q\bar{q}}(r, x)R_g(\lambda), \quad (5.7)$$

in terms of λ given by Eq. (5.6).

In order to study the rapidity distribution of the vector mesons produced in AA UPCs, one needs to incorporate the incoming photon flux $n(\omega)$ in one of the incident nuclei such that

$$\frac{d\sigma^{AA \rightarrow VAA}}{dydt} = n(\omega) \frac{d\sigma^{\gamma A \rightarrow VA}}{dt}(y) + \{y \rightarrow -y\}, \quad (5.8)$$

where $\omega = (M_V/2)e^y$ is the projectile photon energy in the center-of-mass (c.m.) of the colliding particles given in terms of the mass of the vector meson M_V and its rapidity y . The photon flux can be found as [52, 53]

$$n(\omega) = \frac{2Z_A^2 \alpha_{\text{em}}}{\pi} \left\{ \xi K_1(\xi) K_0(\xi) - \frac{\xi^2}{2} [K_1^2(\xi) - K_0^2(\xi)] \right\}, \quad (5.9)$$

where $K_{0,1}$ are the modified Bessel functions of the second kind, Z_A is the charge of the projectile nucleus sourcing the photon flux, $\xi = 2\omega R_A/\gamma$, R_A is the radius of the nucleus (in the numerical analysis below we used R_A value from Ref. [54]), $\gamma = \sqrt{s}/2m_p$ is the Lorentz factor, and m_p is the proton mass.

The gluon density inside a nucleus at small x is expected to be suppressed compared to the one inside a free nucleon caused by a relative reduction of the dipole cross section due to interferences between incoming dipoles in the presence of the higher Fock states of the photon (see e.g. Refs. [23, 48, 55] for more details). This phenomenon also known as the nuclear (or gluon) shadowing effectively reduces the quarkonia photoproduction $\sigma^{\gamma A \rightarrow VA}$ cross section off a heavy nuclear target in comparison to that off the proton, $A\sigma^{\gamma p \rightarrow Vp}$. Such a shadowing effect plays the most important role at central rapidities of the meson, and can be phenomenologically incorporated by ‘‘renormalising’’ the dipole cross section as

$$\sigma_{q\bar{q}}(x, r) \rightarrow \sigma_{q\bar{q}}(x, r)R_G(x, \mu^2), \quad (5.10)$$

where R_G is given in terms of a ratio of the gluon density function inside the heavy nucleus $xg_A(x, \mu^2)$ over the one inside the proton $xg_p(x, \mu^2)$ as

$$R_G(x, \mu^2) = \frac{xg_A(x, \mu^2)}{A xg_p(x, \mu^2)}. \quad (5.11)$$

In practical calculations, we employ the EPPS16 parameterisation for the nuclear gluon distribution fitted to the LHC data [56] adopting $\mu = M_V/2$ as the factorisation scale [57].

Besides the nuclear shadowing effect, there is another important correction to the coherent photoproduction cross section off a nucleus that is worth to be mentioned. In order to obtain the equations above, we used the Glauber-Gribov approach, which takes into account that the inelastic interactions with the nucleons in the target nucleus can produce particles that shortly thereafter can be absorbed by another bound nucleon effectively making the nucleus more transparent. These inelastic corrections are calculated considering that at high energies the dipole is an eigenstate of interaction, with its transverse separation being ‘‘frozen’’ in

the course of its propagation through the target nucleus [58, 59]. This is called the “frozen” approximation and guarantees that there are no fluctuations of the $q\bar{q}$ dipole inside the nucleus. This approximation is only valid if the lifetime of the $q\bar{q}$ state, or the so-called coherence length,

$$l_c = \frac{2\nu}{M_V^2}, \quad (5.12)$$

is much larger than the nuclear radius i.e. $l_c \gg R_A$. Here, ν is the energy of the photon in the nucleus rest frame.

In the case where the coherence length is finite (i.e. when it is not much larger than the nuclear radius ($l_c \lesssim R_A$)), one needs to incorporate additional corrections to the differential cross section $d\sigma^{\gamma A \rightarrow V A}/dt$, which depend on the c.m. energy W . This effect occurs because the photon can propagate through the nucleus without experiencing any attenuation until the $Q\bar{Q}$ fluctuation is produced. This propagation through the nucleus can be described mathematically by a light-cone Green function that satisfies a two-dimensional equation of motion (for more details, see Ref. [60]), whose solution is known only for the quadratic dependence of the dipole cross section approximation $\sigma_{q\bar{q}} \propto r^2$ and for the oscillator form of the interquark potential. In our previous work [30], we used a simplified way to take this effect into account by multiplying the nuclear cross sections in the infinite coherence length limit by a form factor that can be found in Ref. [48]. It has been shown in a recent work of Ref. [61] that such an estimate is valid with a reasonable accuracy only for photoproduction of ρ mesons. So the authors compared the vector dominance model with the approach based on the light-cone Green function and showed that there is a substantial difference between the form factors computed within each approach for small values of energy, mainly for the incoherent case.

The effect of the finite coherence length is known to be sizable only at large values of rapidity, where there are not many measured data points. In this work we are focused on making the predictions for the differential quarkonia photoproduction cross sections at the LHC energies, and we chose to evaluate all the results for $y = 0$. At this value, the finite coherence length effect does not affect the cross section so it can be safely disregarded.

VI. RESULTS FOR γA AND AA COLLISIONS

Now, we would like to present the numerical results for the differential cross sections of coherent vector meson production in γA collisions as well as in AA UPCs. As was described above, in our numerical calculations we employ the potential approach for $1S$ and $2S$ charmonia and bottomonia LF wave functions incorporating the Melosh spin rotation. For the partial dipole amplitude, here we use a numerical solution of the BK equation assuming no angular correlation in the $Q\bar{Q}$ dipole orientation with respect to the color background field of the target nucleus. This is motivated by our observation made above that the BK dipole amplitude provides a better description of the proton target data among a variety of other models we have tested in our approach. The vector meson wave functions are obtained with the Buchmüller-Tye potential while the differences between the results obtained with other potentials appear to be not significant for this analysis. Furthermore, the effects of the nuclear shadowing have been accounted for using a phenomenological approach fitted to data [56].

In Fig. 6 we present predictions for the differential cross section of the $\gamma A \rightarrow V A$ coherent photoproduction of ψ states (left panel) at $W = 100$ GeV and Υ states (right panel) at

$W = 120$ GeV off the lead target. We notice in this figure that the positions of the dips are almost the same for both $\psi(1S, 2S)$ and $\Upsilon(1S, 2S)$, which is caused by the destructive interference of individual scattering amplitudes of the nucleons of the target nucleus.

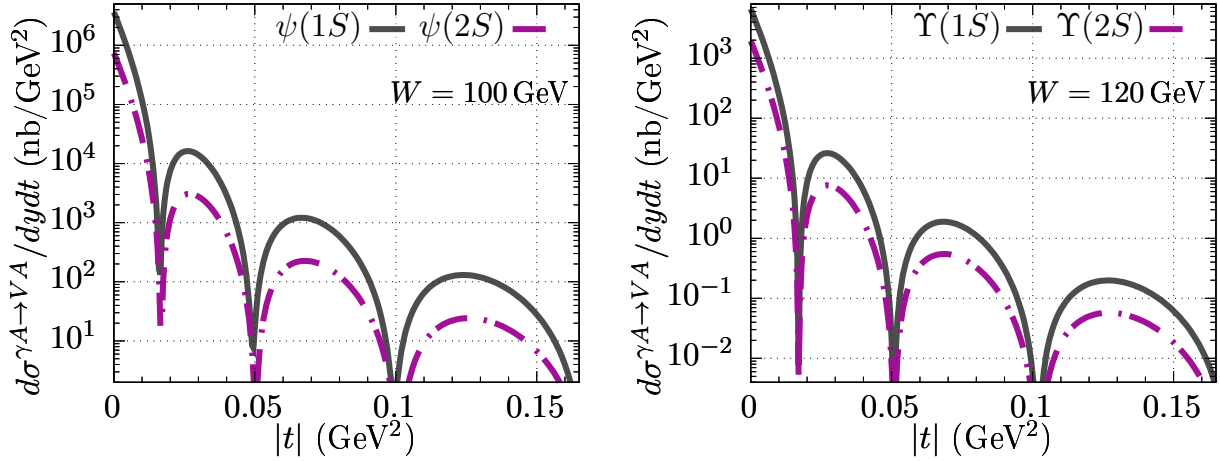


FIG. 6: Predictions for the differential cross sections for $\gamma Pb \rightarrow VPb$ process as functions of $|t|$, calculated with the Buchmüller-Tye potential and with a numerical solution of the BK equation for the dipole amplitude, for the production of ψ states (left) at $W = 100$ GeV and Υ states (right) at $W = 120$ GeV. Both panels present the results at $y = 0$.

In Fig. 7 we present a similar plot but for $AA \rightarrow VAA$ process in AA UPCs for the LHC conditions (with lead nuclei), namely, at $\sqrt{s} = 5.02$ TeV. We also chose central ($y = 0$) rapidity in order to maximise the corresponding differential cross sections and hence to increase the possibility of detection at the LHC. One obvious thing to mention is that these results have exactly the same shape as the ones in Fig. 6, except that they are three orders of magnitude larger, which is caused by the photon flux.

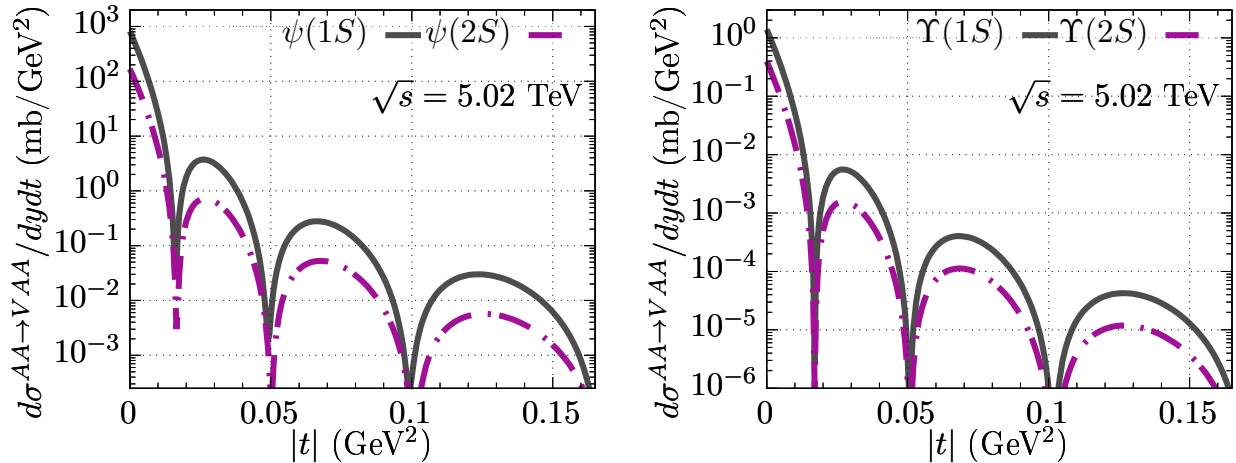


FIG. 7: Predictions for the differential cross sections for $PbPb \rightarrow VPbPb$ process as functions of $|t|$, calculated with the Buchmüller-Tye potential and with numerical solution of the BK equation of Ref. [18] for the dipole amplitude, for production of ψ states (left) and Υ states (right) at $\sqrt{s} = 5.02$ TeV and $y = 0$.

VII. CONCLUSIONS

In this work, the impact-parameter b dependent dipole model has been employed for studies of differential (in momentum transfer squared t) observables of elastic (coherent) quarkonia photoproduction off the proton and nuclear targets. In the treatment of quarkonia Light-Front wave functions, our work relies on the potential approach. Here, a radial-wave solution of the Schrödinger equation for a given interquark potential is first obtained in the $Q\bar{Q}$ rest frame and then boosted to the infinite momentum frame while the spin-dependent part of the wave function is computed by means of the Melosh transformation. We also incorporate the skewness effect in the partial dipole amplitude at the γp level, while in the nuclear case the dipole cross section for an elementary dipole scattering off a single nucleon has been multiplied by such a correction factor, and not the whole γA amplitude. Besides, the gluon shadowing effect in photoproduction off a heavy nucleus target has been accounted for fully phenomenologically.

Using the Buchmüller-Tye potential and a b -dependent solution of the Balitsky-Kovchegov (BK) equation for the dipole-target amplitude, our results reproduce well the H1 data available from the HERA collider for differential J/ψ photoproduction cross section. The same setup has been used to make predictions for the t -dependent photoproduction $\gamma p \rightarrow Vp$ cross section of $\psi(2S)$ meson, as well as for $\Upsilon(1S, 2S)$ states. This is the first prediction using a realistic potential model for the excited-state wave functions and based on the latest developments in the b -dependent BK equation as described above.

Furthermore, new predictions for the differential $\gamma Pb \rightarrow VPb$ and $PbPb \rightarrow VPbPb$ cross sections at central rapidity have been reported for both ground and excited ψ and Υ states. They take into account the Glauber–Gribov picture of high energy scattering and include the gluon shadowing from a recent parametrization of nuclear PDFs. Again, the combination of these ingredients was not done so far in the literature, despite the large importance of each individual one. These are expected to be of large importance for further deeper investigations of the quarkonia coherent photoproduction mechanisms in ultraperipheral collisions in the future measurements at the LHC and at the electron–ion collider [62].

ACKNOWLEDGMENTS

This work was supported by Fapesc, INCT-FNA (464898/2014-5), and CNPq (Brazil) for CH, EGdO, and HT. This study was financed in part by the Coordenação de Aperfeiçoamento de Pessoal de Nível Superior – Brasil (CAPES) – Finance Code 001. The work has been performed in the framework of COST Action CA15213 “Theory of hot matter and relativistic heavy-ion collisions” (THOR). R.P. is supported in part by the Swedish Research Council grants, contract numbers 621-2013-4287 and 2016-05996, as well as by the European Research Council (ERC) under the European Union’s Horizon 2020 research and innovation programme (grant agreement No 668679).

[1] H. Mäntysaari, Rept. Prog. Phys. **83**, 082201 (2020), arXiv:2001.10705 [hep-ph].

[2] S. Glazov (H1), *Proceedings, 36th International Symposium on Multiparticle dynamics (ISMD 2006): Paraty, Brazil, September 2-8, 2006*, Braz. J. Phys. **37**, 793 (2007).

- [3] W. Schäfer, Eur. Phys. J. **A56**, 231 (2020).
- [4] R. Aaij *et al.* (LHCb), JHEP **09**, 084 (2015), arXiv:1505.08139 [hep-ex].
- [5] A. Bursche (LHCb), *Proceedings, 27th International Conference on Ultrarelativistic Nucleus-Nucleus Collisions (Quark Matter 2018): Venice, Italy, May 14-19, 2018*, Nucl. Phys. **A982**, 247 (2019).
- [6] R. Aaij *et al.* (LHCb), JHEP **10**, 167 (2018), arXiv:1806.04079 [hep-ex].
- [7] B. Abelev *et al.* (ALICE), Phys. Lett. **B718**, 1273 (2013), arXiv:1209.3715 [nucl-ex].
- [8] E. Abbas *et al.* (ALICE), Eur. Phys. J. **C73**, 2617 (2013), arXiv:1305.1467 [nucl-ex].
- [9] J. Adam *et al.* (ALICE), Phys. Lett. **B751**, 358 (2015), arXiv:1508.05076 [nucl-ex].
- [10] E. L. Kryshen (ALICE), *Proceedings, 26th International Conference on Ultra-relativistic Nucleus-Nucleus Collisions (Quark Matter 2017): Chicago, Illinois, USA, February 5-11, 2017*, Nucl. Phys. **A967**, 273 (2017), arXiv:1705.06872 [nucl-ex].
- [11] S. Acharya *et al.* (ALICE), Phys. Lett. **B798**, 134926 (2019), arXiv:1904.06272 [nucl-ex].
- [12] V. Khachatryan *et al.* (CMS), Phys. Lett. **B772**, 489 (2017), arXiv:1605.06966 [nucl-ex].
- [13] A. M. Sirunyan *et al.* (CMS), Eur. Phys. J. **C79**, 277 (2019), arXiv:1809.11080 [hep-ex].
- [14] H. Kowalski, L. Motyka, and G. Watt, Phys. Rev. **D74**, 074016 (2006), arXiv:hep-ph/0606272 [hep-ph].
- [15] I. Balitsky, Nucl. Phys. B **463**, 99 (1996), arXiv:hep-ph/9509348.
- [16] Y. V. Kovchegov, Phys. Rev. D **61**, 074018 (2000), arXiv:hep-ph/9905214.
- [17] B. Ducloué, E. Iancu, G. Soyez, and D. N. Triantafyllopoulos, Phys. Lett. **B803**, 135305 (2020), arXiv:1912.09196 [hep-ph].
- [18] D. Bendova, J. Cepila, J. G. Contreras, and M. Matas, Phys. Rev. **D100**, 054015 (2019), arXiv:1907.12123 [hep-ph].
- [19] J. Cepila, J. G. Contreras, and M. Matas, (2020), arXiv:2002.11056 [hep-ph].
- [20] Y. Hatta, B.-W. Xiao, and F. Yuan, Phys. Rev. Lett. **116**, 202301 (2016).
- [21] B. Z. Kopeliovich, L. I. Lapidus, and A. B. Zamolodchikov, JETP Lett. **33**, 595 (1981), [Pisma Zh. Eksp. Teor. Fiz.33,612(1981)].
- [22] N. N. Nikolaev and B. G. Zakharov, J. Exp. Theor. Phys. **78**, 598 (1994), [Zh. Eksp. Teor. Fiz.105,1117(1994)].
- [23] B. Z. Kopeliovich and B. G. Zakharov, Phys. Rev. **D44**, 3466 (1991).
- [24] B. Z. Kopeliovich, J. Nemchick, N. N. Nikolaev, and B. G. Zakharov, Phys. Lett. **B324**, 469 (1994), arXiv:hep-ph/9311237 [hep-ph].
- [25] J. Nemchik, N. N. Nikolaev, and B. G. Zakharov, Phys. Lett. **B341**, 228 (1994), arXiv:hep-ph/9405355 [hep-ph].
- [26] J. Nemchik, N. N. Nikolaev, E. Predazzi, and B. G. Zakharov, Z. Phys. **C75**, 71 (1997), arXiv:hep-ph/9605231 [hep-ph].
- [27] M. B. G. Ducati, M. T. Griep, and M. V. T. Machado, Phys. Rev. **C88**, 014910 (2013), arXiv:1305.2407 [hep-ph].
- [28] J. Hufner, Yu. P. Ivanov, B. Z. Kopeliovich, and A. V. Tarasov, Phys. Rev. **D62**, 094022 (2000), arXiv:hep-ph/0007111 [hep-ph].
- [29] A. Shuvaev, K. J. Golec-Biernat, A. D. Martin, and M. Ryskin, Phys. Rev. D **60**, 014015 (1999), arXiv:hep-ph/9902410.
- [30] C. Henkels, E. G. de Oliveira, R. Pasechnik, and H. Trebien, Phys. Rev. D **102**, 014024 (2020), arXiv:2004.00607 [hep-ph].
- [31] A. Martin, Phys. Lett. **93B**, 338 (1980).
- [32] N. Barik and S. N. Jena, Phys. Lett. **97B**, 265 (1980).

- [33] E. Eichten, K. Gottfried, T. Kinoshita, K. D. Lane, and T.-M. Yan, Phys. Rev. **D17**, 3090 (1978), [Erratum: Phys. Rev.D21,313(1980)].
- [34] E. Eichten, K. Gottfried, T. Kinoshita, K. D. Lane, and T.-M. Yan, Phys. Rev. **D21**, 203 (1980).
- [35] W. Buchmuller and S. H. H. Tye, Phys. Rev. **D24**, 132 (1981).
- [36] C. Quigg and J. L. Rosner, Phys. Lett. **71B**, 153 (1977).
- [37] H. J. Melosh, Phys. Rev. **D9**, 1095 (1974).
- [38] M. Krelina, J. Nemchik, R. Pasechnik, and J. Cepila, Eur. Phys. J. **C79**, 154 (2019), arXiv:1812.03001 [hep-ph].
- [39] J. Cepila, J. Nemchik, M. Krelina, and R. Pasechnik, Eur. Phys. J. C **79**, 495 (2019), arXiv:1901.02664 [hep-ph].
- [40] S. Dulat, T.-J. Hou, J. Gao, M. Guzzi, J. Huston, P. Nadolsky, J. Pumplin, C. Schmidt, D. Stump, and C. Yuan, Phys. Rev. D **93**, 033006 (2016), arXiv:1506.07443 [hep-ph].
- [41] H. Kowalski and D. Teaney, Phys. Rev. D **68**, 114005 (2003), arXiv:hep-ph/0304189.
- [42] E. Iancu, J. Madrigal, A. Mueller, G. Soyez, and D. Triantafyllopoulos, Phys. Lett. B **750**, 643 (2015), arXiv:1507.03651 [hep-ph].
- [43] S. Drell and T.-M. Yan, Phys. Rev. Lett. **24**, 181 (1970).
- [44] S. J. Brodsky and G. R. Farrar, Phys. Rev. Lett. **31**, 1153 (1973).
- [45] G. B. West, Phys. Rev. Lett. **24**, 1206 (1970).
- [46] C. Alexa *et al.* (H1), Eur. Phys. J. C **73**, 2466 (2013), arXiv:1304.5162 [hep-ex].
- [47] A. Aktas *et al.* (H1), Eur. Phys. J. **C46**, 585 (2006), arXiv:hep-ex/0510016 [hep-ex].
- [48] Yu. P. Ivanov, B. Z. Kopeliovich, A. V. Tarasov, and J. Hüfner, Phys. Rev. **C66**, 024903 (2002), arXiv:hep-ph/0202216 [hep-ph].
- [49] Y.-P. Xie and X. Chen, Nucl. Phys. A **959**, 56 (2017), arXiv:1805.05901 [hep-ph].
- [50] R. D. Woods and D. S. Saxon, Phys. Rev. **95**, 577 (1954).
- [51] H. Euteneuer, J. Friedrich, and N. Vogler, Nucl. Phys. **A298**, 452 (1978).
- [52] C. F. von Weizsacker, Z. Phys. **88**, 612 (1934).
- [53] E. J. Williams, Phys. Rev. **45**, 729 (1934).
- [54] H. De Vries, C. De Jager, and C. De Vries, Atom. Data Nucl. Data Tabl. **36**, 495 (1987).
- [55] Y. P. Ivanov, B. Z. Kopeliovich, A. V. Tarasov, and J. Hüfner, *Hadron physics: Effective theories of low energy QCD. Proceedings, 2nd International Workshop, Coimbra, Portugal, September 25-29, 2002*, AIP Conf. Proc. **660**, 283 (2003), arXiv:hep-ph/0212322 [hep-ph].
- [56] K. J. Eskola, P. Paakkinen, H. Paukkunen, and C. A. Salgado, Eur. Phys. J. **C77**, 163 (2017), arXiv:1612.05741 [hep-ph].
- [57] V. Guzey, E. Kryshen, and M. Zhalov, Phys. Rev. C **93**, 055206 (2016), arXiv:1602.01456 [nucl-th].
- [58] B. Kopeliovich, I. Potashnikova, and I. Schmidt, Phys. Rev. C **73**, 034901 (2006), arXiv:hep-ph/0508277.
- [59] B. Kopeliovich, Int. J. Mod. Phys. A **31**, 1645021 (2016), arXiv:1602.00298 [hep-ph].
- [60] B. Kopeliovich, J. Nemchik, A. Schafer, and A. Tarasov, Phys. Rev. C **65**, 035201 (2002), arXiv:hep-ph/0107227.
- [61] B. Kopeliovich, M. Krelina, J. Nemchik, and I. Potashnikova, (2020), arXiv:2008.05116 [hep-ph].
- [62] A. Accardi *et al.*, Eur. Phys. J. A **52**, 268 (2016), arXiv:1212.1701 [nucl-ex].
- [63] A. H. Rezaeian and I. Schmidt, Phys. Rev. **D88**, 074016 (2013), arXiv:1307.0825 [hep-ph].
- [64] A. Łuszczak and W. Schäfer, Phys. Rev. C **99**, 044905 (2019), arXiv:1901.07989 [hep-ph].

- [65] C. A. Flett, A. D. Martin, M. G. Ryskin, and T. Teubner, (2020), arXiv:2006.13857 [hep-ph].
- [66] Y. Ivanov, B. Kopeliovich, and I. Schmidt, in *Workshop on Heavy Ion Collisions at the LHC: Last Call for Predictions* (2007) arXiv:0706.1532 [hep-ph].
- [67] D. Bendova, J. Cepila, J. Contreras, and M. Matas, (2020), arXiv:2006.12980 [hep-ph].
- [68] H. Mäntysaari and B. Schenke, Phys. Lett. B **772**, 832 (2017), arXiv:1703.09256 [hep-ph].
- [69] T. Toll and T. Ullrich, Phys. Rev. C **87**, 024913 (2013), arXiv:1211.3048 [hep-ph].